FASEB BioAdvances **WILEY**

Fluorescent identification of axons, dendrites and soma of neuronal retinal ganglion cells with a genetic marker as a tool for facilitating the study of neurodegeneration

Puttipong Sripinun[1,2,3] | Wennan Lu[1] | Sergei Nikonov[4] | Suhani Patel[1] |
Sarah Hennessy[1] | Tianyuan Yao[5,6] | Qi N. Cui[5] | Brent A. Bell[5] |
Claire H. Mitchell[1,7]

[1]Department of Basic and Translational Science, University of Pennsylvania, Philadelphia, Pennsylvania, USA

[2]Department of Orthodontics, University of Pennsylvania, Philadelphia, Pennsylvania, USA

[3]Department of Orthodontics and Pediatric Dentistry, Chiang Mai University, Chiang Mai, Thailand

[4]Department of Neuroscience, University of Pennsylvania, Philadelphia, Pennsylvania, USA

[5]Department of Ophthalmology, University of Pennsylvania, Philadelphia, Pennsylvania, USA

[6]College of Medicine, University of Arkansas for Medical Sciences, Little Rock, Arkansas, USA

[7]Department of Physiology, University of Pennsylvania, Philadelphia, Pennsylvania, USA

Correspondence
Claire H. Mitchell, Department of Basic and Translational Science, University of Pennsylvania, 440 Levy Building, 240 S. 40th St, Philadelphia, PA 19104, USA.
Email: chm@upenn.edu

Abstract

This study characterizes a fluorescent *Slc17a6*-tdTomato neuronal reporter mouse line with strong labeling of axons throughout the optic nerve, of retinal ganglion cell (RGC) soma in the ganglion cell layer (GCL), and of RGC dendrites in the inner plexiform layer (IPL). The model facilitated assessment of RGC loss in models of degeneration and of RGC detection in mixed neural/glial cultures. The td-Tomato signal showed strong overlap with >98% cells immunolabeled with RGC markers RBPMS or BRN3A, consistent with the ubiquitous presence of the vesicular glutamate transporter 2 (VGUT2, SLC17A6) in all RGC subtypes. There was no cross-labeling of ChAT-positive displaced amacrine cells in the GCL, although some signal emanated from the outer plexiform layer, consistent with horizontal cells. The fluorescence allowed rapid screening of RGC loss following optic nerve crush and intraocular pressure (IOP) elevation. The bright fluorescence also enabled non-invasive monitoring of extensive neurite networks and neuron/astrocyte interactions in culture. Robust Ca^{2+} responses to P2X7R agonist BzATP were detected from fluorescent RGCs using Ca^{2+}-indicator Fura-2. Fluorescence from axons and soma was detected in vivo with a confocal scanning laser ophthalmoscope (cSLO); automatic RGC soma counts enhanced through machine learning approached the numbers found in retinal wholemounts. Controls indicated no impact of *Slc17a6*-tdTomato expression on light-dependent neuronal function as measured with a microelectrode array (MEA), or on retinal structure as measured with optical coherence tomography (OCT). In summary, the bright fluorescence in axons, dendrites and soma of ~all RGCs in the *Slc17a6*-tdTomato reporter mouse may facilitate the study of RGCs.

KEYWORDS

axons, dendrites, glial/neuron culture, IOP, machine learning, MEA, neurodegeneration, optic nerve crush, RBPMS, retinal ganglion cells, *Slc17a6*-tdTomato, VGLUT2

1 | INTRODUCTION

Retinal ganglion cells (RGCs) integrate retinal activity to generate action potentials and thus transmit the visual message to the brain along the optic nerve.[1,2] RGCs are particularly susceptible to damage and loss in diseases such as glaucoma, optic neuritis, ischemic optic neuropathy, and diabetic retinopathy.[3–6] The screening of treatments to prevent RGC loss is an active field of research, and enhanced approaches to identify RGCs within the retina and in the optic nerve could facilitate screening.

Several techniques have been developed for identifying RGCs, including fluorescence imaging of retrograde tracer labeling, intravitreal tracer labeling, and post-mortem immunohistochemical staining; each has its advantages and drawbacks.[7] Retrograde and intravitreal tracer labeling have led to many advances, but only a portion of RGCs are labeled and the surgery required to deliver the tracer can itself cause tissue damage.[8] While immunohistochemical staining of RGCs has improved with antibodies to targets such as RPBMS and BRN3A, their detection in only the soma or nucleus, respectively, limits their impact. The requirement for multistep immunohistochemical processing, often including fixation, also reduces their usefulness.

Strains of fluorescent reporter mice can address some of these concerns. The development of *Thy1*-XFP reporter mice to express fluorescent proteins in RGCs represented a considerable advance, as the approach was less invasive and longer lasting.[9] However, expression of the *Thy1* promoter is limited to certain RGC subtypes, and *Thy1*-YFP or *Thy1*-CFP are expressed in only ~60%–80% RGCs.[10–13] Furthermore, the transgene has also been detected on some amacrine, bipolar, and Müller cells, complicating quantification of RGCs.[9,12,14,15] CRISPR- Cas9 modified *Brn3b*-mCherry mice had a fluorescent signal in 71% of RPBMS+ cells, as expected based on the proportion of BRN3B cells in total.[16] The *RBPMS*[CreERT2-tdTomato] mice recently developed show improved specificity, although incomplete penetrance of tamoxifen treatment may contribute to the labeling of only a portion of RGCs with fluorescence.[17]

The *Slc17a6* driven-promotor is emerging as a promising candidate for pan-RGCs populational studies. The *Slc17a6* gene codes for the vesicular glutamate uptake transporter 2 (VGLUT2), and single-cell analysis detected expression of *Slc17a6* in all 45 molecular clusters corresponding to distinct RGC subtypes.[18] Earlier studies demonstrated increasing immunoreactivity to VGLUT2 in the ganglion cell layer starting from P0 and extending throughout all developmental stages into the adult.[19] A single-cell RNA-sec study identified *Slc17a6* in RGCs but not amacrine cells,[20] while ubiquitous expression of *Slc17a6* in all RGC subtypes was reported using Cre-reporter mice, with moderate expression in horizontal cells and some cones suggested.[21,22] A more thorough characterization of *Slc17a6*-reporter mice is necessary to highlight their potential and identify limitations.

This study undertook a systematic characterization of the *Slc17a6*-driven tdTomato transgenic mouse as a promising candidate for the study of RGCs. Robust expression of tdTomato was detected in RGC soma, and in axons along the nerve fiber layer, optic nerve head, and myelinated optic nerve. Dendrites were detected from soma projecting into the inner plexiform layer (IPL) when mice were examined with two-photon microscopy. The specificity of tdTomato fluorescence was analyzed with co-staining for known RGC and amacrine cell markers. Controls evaluating the impact of the model on electrical activity of RGCs and on retinal structure indicated there were no gross changes. Two disease models demonstrated the application of this transgenic line to the study of RGC degeneration. The retention of fluorescence in cultured RGCs in vitro was demonstrated and used to monitor the growth of RGC neurites in mixed retinal cultures over several weeks. In vivo imaging suggested the potential future use of the mouse for non-invasive screening when used in conjunction with machine learning. Overall, this study emphasized the potential of the *Slc17a6*-tdTomato mouse to facilitate the study of the physiology and pathophysiology of RGCs.

2 | METHODS

2.1 | Animal care and use

All experimental protocols were performed in accordance with the NIH Guide for the Care and Use of Experimental Animals and approved by the Institutional Animal Care and Use Committee of the University of Pennsylvania (IACUC). *Slc17a6*-driven Cre (*Slc17a6*[Cre+/+]; RRID:IMSR_JAX:028863) and Ai9 mice (*R26R*[tdTomato]; RRID:IMSR_JAX:007909), acquired from the Jackson Laboratory (Bar Harbor, ME, USA), were used to generate tdTomato-labeled RGCs mice (*Slc17a6*[Cre+]; *R26R*[tdTomato+]) (Figure S1). Mice were socially housed and bred in cages with regular corn bedding under standard conditions with 12-h day/night cycles and ambient humidity rooms, with food and water and libitum as described.[23]

2.2 | Immunohistochemistry

Transcardiac perfusion with phosphate buffered saline (PBS) and 4% paraformaldehyde was performed on mice anesthetized and maintained with 1.5% isoflurane

throughout the procedure. Dissected eyes were post-fixed with 4% paraformaldehyde and cryoprotected in 30% sucrose overnight at 4°C, followed by embedding in optimal cutting temperature compound. Retinal whole-mounts or 10 μm sections were fixed with 4% paraformaldehyde for 10 min, permeabilized with 0.1% Triton X-100 and 20% SuperBlock buffer (ThermoFisher, Waltham, MA) in 0.1% PBS-T for 10–30 min at 25°C, then blocked with 10% donkey serum and 20% SuperBlock in PBS-T for 1 h, followed by primary antibodies 24–48 h at 4°C. Primary antibodies were raised against BRN3A (1:50 dilution; Millipore Cat# MAB1585, RRID:AB_94166), RBPMS (1:200 dilution; GeneTex Cat# GTX118619, RRID:AB_10720427), Beta-tubulin III (1:200 dilution; BioLegend Cat# 801212, RRID:AB_2721321), GFAP (1:200 dilution, Abcam Cat# Ab53554, RRID:AB_880202), and Choline Acetyltransferase (1:100 dilution; PhosphoSolutions Cat# 315-CHAT, RRID:AB_2492055). Retinal wholemounts or sections were then washed with 0.1% PBS-T and incubated with appropriate secondary antibodies conjugated to Alexa Fluor 488, 568, or 647 (1:500 dilution; Invitrogen ThermoFisher). After incubation with 4′,6-diamidino-2-phenylindole (DAPI), slides were mounted with SlowFade Gold antifade reagent (ThermoFisher). Imaging was performed using a Nikon Eclipse Ti2- microscope with a Crestor spinning disk confocal system and analyzed using NIS Elements Imaging software v. 4.60 (Nikon Instruments, Melville, NY).

2.3 | Retinal ganglion cell counts in vitro

RGC counts were determined from images of *Slc17a6*-tdTomato mice with or without antibody staining. While soma could be identified distal the bright fluorescence of the nerve fiber layer using z-stack layering of confocal microscopy, this did complicate the analysis, so quantification was performed in regions 700–800 μm from the optic nerve head where the concentration of nerve fibers was less. Images were obtained from superior, inferior, temporal and nasal quadrants, and counted manually. Some of the images were counted independently by two separate observers; the close correlation of their manual counts supported the accuracy of the determination (Figure S2).

2.4 | Two-photon imaging

Mice were euthanized by CO_2 inhalation followed by cervical dislocation. Eyes were enucleated and dissected in Ames solution (Sigma-Aldrich) at room temperature and continuously oxygenated with a mixture of 95% O_2 and 5% CO_2. Retinas were flat-mounted with ganglion cells side up in a recording chamber perfused with the same solution maintained at 37°C using a TC-344C two-channel temperature controller (Warner Instruments, Holliston, MA, USA). All procedures were performed under dim-red light. Two-photon imaging using an Olympus FV1000 MPE Multiphoton Laser Scanning Microscope (Olympus, Center Valley, PA, USA) was employed, with the wavelength for two-photon excitation set at 1000 nm.

2.5 | Mouse models of retinal ganglion cell damage

Optic nerve crush surgery was performed based on standard approaches.[24] In brief, mice were anesthetized and maintained with 1.5% isoflurane throughout the procedure after receiving 5 mg/kg meloxicam. The temperature was maintained using a heating pad. Under a dissecting microscope, a small incision was made on the superolateral conjunctiva, and blunt dissection completed with fine forceps (World Precision Instruments) to expose the optic nerve. The optic nerve was clamped with microforceps (World Precision Instruments) 1–2 mm behind the globe. After the crush injury procedure, a triple-antibiotic ointment (neomycin/polymyxin B sulfates/bacitracin zinc ophthalmic ointment) was applied to the surgical site, and mice were closely monitored for signs of discomfort. Mice were sacrificed after 7 days, and RGC counts from control and contralateral crush retinal wholemounts were performed as described above.

A transient IOP elevation procedure was modified from the Controlled Elevation of IOP (CEI) approach developed by Morrison and colleagues and the transient method of Crowson and colleagues, as described.[25–27] In brief, mice were continuously anesthetized with 1.5% isofluorane and treated with proparacaine (0.5%) and tropicamide (0.5%–1%). The anterior chamber of one eye was cannulated with a 33-gauge needle attached to polyethylene tubing (PE 50; Becton Dickinson) connected to a 20 mL syringe filled with sterile Hanks Buffered Saline Solution (HBSS). The IOP was increased to 58–60 mmHg by elevating the reservoir to the appropriate height. IOP was returned to baseline after 4 h, the needle removed, and antibiotic ointment was applied to the cornea. Retinal tissues were isolated for counts of fluorescent RGCs 10 days after IOP elevation.

2.6 | Retinal ganglion cells in mixed retinal cell culture

Mixed retinal cells were cultured from mouse pups aged P4-6 using an improved approach to support more elaborate RGC growth over longer durations as compared

to previous culture protocols.[28] Immediately following euthanasia, isolated retinas were treated with papain (16.5 U/mL; Cat# LK003176; Worthington) and DNase I (12,500 U/mL; Cat# LK003170; Worthington) for 30 min at 37°C. The cells were gently triturated and plated on a 12 mm Nunc glass base dish (Cat# 150680; Thermo Scientific) coated with poly-D-lysine and mouse laminin I. RGC culture media was adapted from published reports[29]; it contained a mix of DMEM (Cat# 11960044; Gibco) and neurobasal media (Cat# 21103049; Gibco), with insulin (5 μg/mL; Cat# I6634; Sigma), sodium pyruvate (1 mM; Cat# 11360–070; Sigma), NS21 supplement (Cat# AR008; R&D systems), penicillin/streptomycin (1%, Cat # 15140–12; Gibco), SATO supplement (1X; made in house containing Neurobasal Medium (Invitrogen), bovine serum albumin (100 μg/mL; Sigma, A4161), sodium selenite (40 ng/mL), putrescine (16 μg/mL), triiodo-thyronine (1.6 μg/mL), apo-transferrin (100 μg/mL; Sigma, T-1147), and progesterone (60 ng/mL) as described),[30] L-glutamine (2 mM, Cat# 25030–081; Gibco), triiodothyronine (T3, 40 ng/mL, Cat# T6397; Sigma), brain-derived neurotrophic factor (BDNF; 50 ng/mL; Cat# 450–02; Peprotech, Rocky Hill, NJ), ciliary neurotrophic factor (CNTF; 10 ng/mL; Cat# 450–13; Peprotech), and forskolin (4.2 ng/mL; Cat# F6886; Sigma Aldrich). RGCs continued to grow for at least 4 weeks, when monitoring stopped; neurite growth and soma numbers were monitored daily from live cultures with an inverted Nikon Eclipse tissue culture microscope with a TRITC filter set (544 nm excitation/570 nm emission), and images captured with a color DSFi1 camera (all Nikon Instruments).

2.7 | Ca²⁺ measurement from retinal ganglion cells

Levels of intracellular Ca^{2+} in RGCs were determined microscopically based on approaches described previously.[28,31] In brief, mixed retinal cultures 3–5 days after plating were loaded with 5 μM Fura-2 AM (Thermo Fisher) with 0.01% pluronic F-127 at 37°C for 45 min. Cells were washed, mounted in a perfusion chamber, and visualized using a ×40 objective on a Nikon Diaphot microscope. Ratiometric measurements were performed by alternating the excitation wavelength from 340 to 380 nm and quantifying emission ≥512 nm with a charge-coupled device camera (All Photon Technologies International, Lawrenceville, NJ, USA). Cells were perfused with isotonic solution containing 105 mM NaCl, 5 mM KCl, 6 mM 4-(2-hydroxyethyl)-1-piperazineethanesulfonic (HEPES) acid, 4 mM NaHEPES, 5 mM NaHCO₃, 60 mM mannitol, 5 mM glucose, and 1.3 mM CaCl₂. The P2X7R agonist Benzoylbenzoyl-ATP

(BzATP; Cat# B6396, Sigma) was added to the perfusate for the time indicated as a positive control given its well-documented ability to stimulate RGCs.[32,33]

2.8 | *In vivo* imaging system and analysis

Non-invasive retinal imaging was conducted utilizing confocal scanning laser ophthalmoscopy (cSLO, Spectralis HRA, Heidelberg Engineering), ultra-high resolution spectral-domain optical coherence tomography (SD-OCT, Envisu R2200 UHR, Bioptigen) and Micron3 fluorescent retinal imaging (Pheonix-Micron Inc., Bend, OR) in the University of Pennsylvania Small Animal Ocular Imaging facility, as previously described.[34] A 2:1 pupil dilation mixture of 2.5% phenylephrine and 1% tropicamide was applied to both eyes of the mouse, followed by induction of anesthesia using intraperitoneal injection of a combination of ketamine and xylazine (Dechra Veterinary Products, Overland Park, KS). Ocular protection against evaporative corneal desiccation during imaging involved using artificial tears (Refresh, Irvine, CA) and ocular eye shields. SD-OCT was performed to examine the retinal structure with a 45°–51° FOV (~1.4 mm) with the optic nerve centrally positioned. Puralube Vet Ointment (Dechra Veterinary Products) was applied to the corneas to protect eyes during recovery.

For cSLO image acquisition, *Slc17a6*-tdTomato mice were imaged with the Ultra-wide Field (UWF) 105° objective lens using a digital zoom of 51°. Blue-autofluorescence (BAF-cSLO; 488 nm excitation/500 long pass emission) images were collected in High-resolution using either a 102° (1536×1536 pixels) or 51° (768×768) Field of view (FOV) with the optic disk centrally positioned within the image. Images captured were automatically co-registered and averaged over 25 individual frames using the Automated Real-time (ART) feature on the instrument. Images were exported as uncompressed TIFF files to ImageJ v1.53e for post-processing. Images were imported and converted from 8-bit RGB to 8-bit grayscale. Image contrast and detail was enhanced by slightly increasing contrast, followed by image sharpening and despeckle noise filtering. Images were then loaded into Ilastik v1.3.3 and processed for Cell Density Counting.[35] All features were selected (Color/Intensity, Edge, and Texture) within Feature Selection. For the machine learning algorithm training, several RGCs were selected within the image using a Foreground Sigma of two. A Background Sigma of one was chosen in between RGCs for 10° images and over the retinal vasculature and bright axons near the optic nerve for the 51° FOV. Cell density counts were then obtained using a Random Forest algorithm (10 trees and 50 max depth). Cell density was calibrated assuming the optic disk was ~0.225 mm in diameter.[36]

2.9 | Microelectrode array recordings

Microelectrode array (MEA) recordings were conducted using established methods on *Slc17a6*-tdTomato and C57BL/6J mice dark-adapted for over 2h as described.[37] Retinal sections were placed ganglion cell layer down in the MEA recording chamber (60MEA200/30iR-Ti-gr; Multi Channel Systems) of a 60-channel MEA system and mounted on the 1060i amplifier (Multi Channel Systems, Reutlingen, Germany). Gentle suction was applied to the sample through perforations in the chamber bottom to enhance its contact with the electrodes, resulting in improved signal quality. The retinal tissue was perfused with oxygenated Ames solution (Sigma–Aldrich) maintained at 37°C, and stimulated with a calibrated series of 455 nm light flashes. Each series included 10 2-s flashes of the same intensity delivered at 0.1 Hz. Different light intensities were used for different stimulation series. Data capture was acquired by an NI PCI-6071E DAQ board and custom software developed in LabView (National Instruments, Austin, TX, USA) and later analyzed using a MATLAB-based custom coding algorithm (MATLAB, Natick, MA, USA).

2.10 | Materials and data analysis

All compounds were obtained from Sigma-Aldrich Inc. (St. Louis, MO) unless otherwise indicated. Statistical analysis was performed using GraphPad Prism software version 10 (GraphPad, San Diego, CA, USA). Significant differences between the two related groups were assessed using an unpaired Student's *t*-test, or with a paired Student's *t*-test to compare contralateral eyes from the same animal. A one-way or two-way ANOVA test was performed when comparing more than two different variables with the appropriate post-hoc test as listed. Pearson's correlation analysis was performed using Graph Pad. All data are presented as mean ± standard deviation. S and significance is shown as ns > 0.05, * $p < 0.05$, ** $p < 0.01$, *** $p < 0.001$, and **** $p < 0.0001$. Results returning $p < 0.05$ were considered significant.

3 | RESULTS

3.1 | Characterization of tdTomato expression in tdTomato-labeled RGCs using Slc17a6-driven Cre recombinase transgenic mouse retina

A bright fluorescent signal was readily apparent in the inner retina from *Slc17a6*[Cre+]; R26R[tdTomato+] (*Slc17a6*-tdTomato) mice. The pattern of tdTomato expression in transverse sections was characterized by bright fluorescence in round cell bodies in the ganglion cell layer (GCL), strands throughout the nerve fiber layer (NFL), and a lighter particulate signal extending into the inner plexiform layer (IPL) (Figure 1A, top). The cellular identity of tdTomato-positive cells in the GCL was confirmed with RGC-specific markers. In the nerve fiber layer, tdTomato fluorescence colocalized with immunostaining for beta-tubulin III, a neural-specific microtubulin protein present in RGCs.[38] The RNA-binding protein RBPMS is a selective marker for RGCs found primarily in the cell body[39]; the tdTomato signal colocalized with immunostaining for RPBMS in the RGC soma.

Colocalization between the tdTomato signal and beta-tubulin III immunofluorescence was present in RGC axons throughout the optic nerve head (Figure 1A, middle). A robust tdTomato signal was also observed throughout the myelinated optic nerve (Figure 1A, bottom). *Slc17a6*-tdTomato mice displayed robust fluorescence across the flat retinal wholemount in both individual cell bodies and axon bundles. The signal was absent in wholemounts from control mice missing the Slc17a7 Cre construct (*Slc17a6*[Cre-]; R26R[tdTomato+]; Figure 1B).

To better examine the fluorescent signals radiating from the soma, two-photon microscopy was used on retinal wholemounts from *Slc17a6*-tdTomato mice. Close inspection identified numerous thin, fluorescent extensions emanating from the soma, consistent with dendrites (Figure 1C, top). Reconstruction of the stacked images into the z-plane indicated the dendrites could be detected as they extended into the IPL ((Video S1).

While the predominant signal from *Slc17a6*-tdTomato mice was in the inner retina, some fluorescence was also observed in a population of cells in the outer plexiform layer (Figure 1D). This is consistent with the expression of *Slc17a6* in a small number of horizontal cells, as previously identified by co-labeling with calbindin.[22,40]

3.2 | Slc17a6 Cre-driven tdTomato expression labeled ~all RGCs but not amacrine cells

As RGCs were the primary focus of our study, a quantitative analysis of the relationship between tdTomato-positive cells, specifically in the GCL, was undertaken with specific pan-RGC markers (Figure 2A,B). All (98.93 ± 1.4%) of the RBPMS-positive cells were also labeled with tdTomato fluorochrome. Quantification indicated 4268 ± 805 tdTom+ cells per mm^2 and 4190 ± 773 RPBMS+ cells per mm^2 (not significantly different, $p = 0.914$). The RGC-specific transcription BRN3A factor is reported to be expressed in ~90% of RGCs[41]; our study

(A)

(B)

(C)

(D)
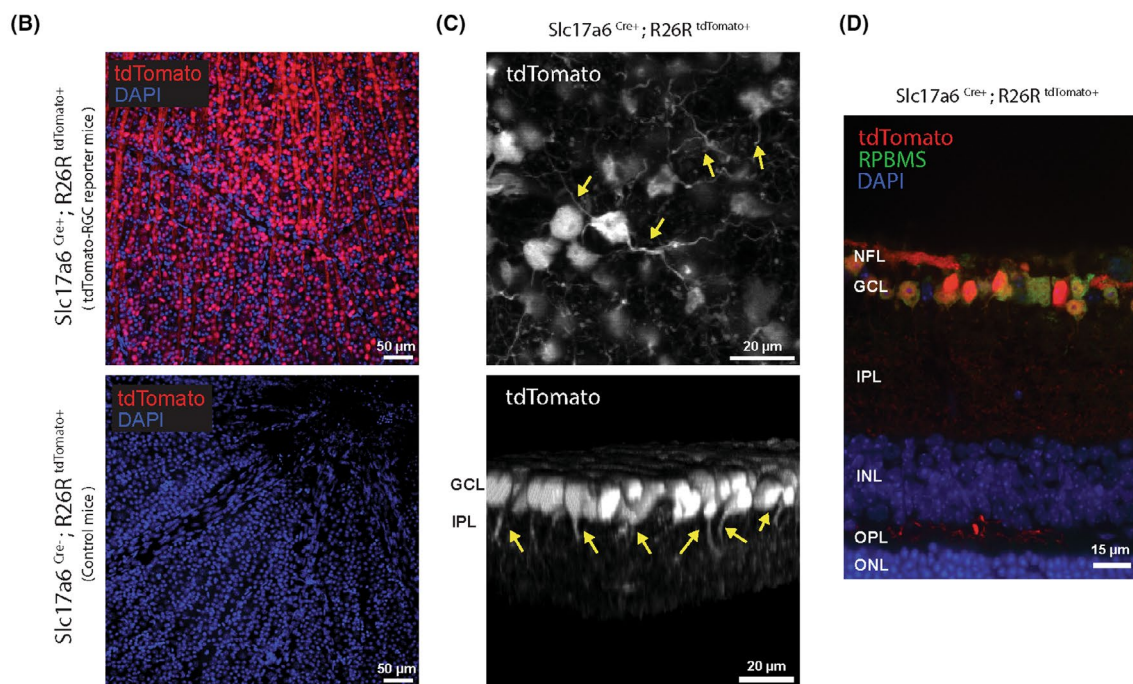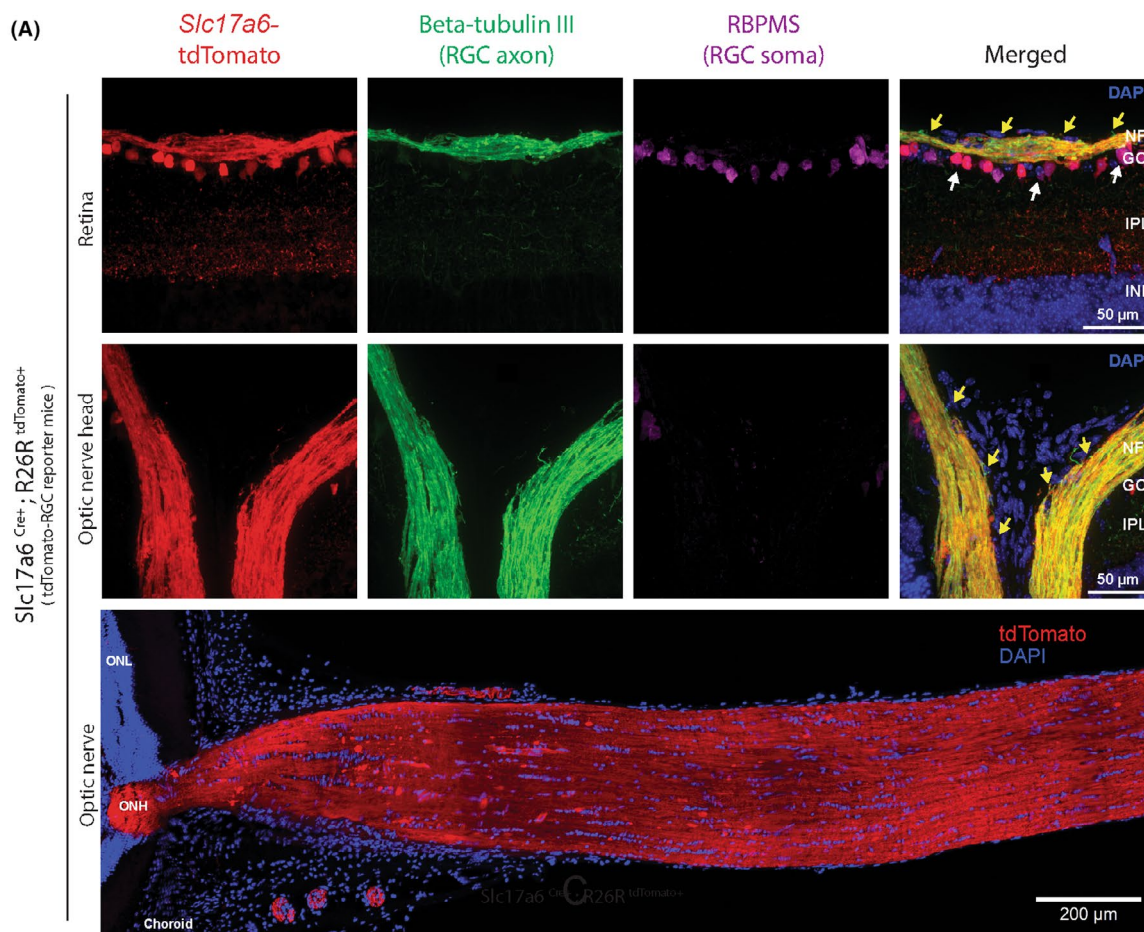
found $88.65 \pm 4.4\%$ of the tdTomato-positive cells also immunostained for BRN3A. Moreover, all $(100 \pm 0.0\%)$ of BRN3A-positive cells also expressed tdTomato expression. Quantification indicated 4311 ± 947 tdTom+ cells per mm^2 and 3837 ± 898 BRN3A+ cells per mm^2 (not significantly different, $p = 0.095$).

While ~all of the RPBMS-and BRN3a positive cells also showed tdTomato fluorescence, the magnitude of

FIGURE 1 tdTomato-labeled *Slc17a6*-driven Cre recombinase expression characteristics in the somas, axons, and dendrites of retinal ganglion cells. (A) Overlap of tdTomato fluorescence with immunofluorescence for retinal ganglion cell markers beta-tubulin III and RPBMS confirmed tdTomato expression in the nerve fiber layer (NFL) and RGC soma in the ganglion cell layer (GCL) (top panel; white arrows). TdTomato fluorescence overlapped with beta-tubulin III along axons through the optic nerve head (middle panel; yellow arrows). The fluorescent signal was also detected throughout the optic nerve after exiting the globe (bottom panel). (B) Cre recombinase drives expression of the tdTomato reporter gene in RGCs (*Slc17a6*[Cre+]; R26R[tdTomato+]), labeling soma and axons in a retinal wholemount. No signal was detected in Cre⁻ mice. (C) Representative 2-photon images of tdTomato-expressing RGCs indicating the presence of dendrites (yellow arrows). Analysis in the *z*-axis suggested the extension of dendrites from the GCL to the inner plexiform layer (IPL, bottom). (D) While not as prevalent as the signal in the GCL, fluorescence was present in the outer plexiform layer (OPL), consistent with horizontal cells.

the fluorescent signal varied somewhat between cells. A correlation between the magnitude of the tdTomato signal and cell size or location was not detected, nor between fluctuations in the strength of the signal from the BRN3A or RPBMS immunostaining. Previous studies found that the expression of *Slc17a6* did vary across RGC subtypes.[18,20] Regardless of the intensity, the tight correlation between immunostaining for RGC markers and fluorescence in the *Slc17a6*-tdTomato mouse suggests the *Slc17a6* Cre-driven tdTomato is expressed to some degree by ~all RGCs.

Previous reporter strains showed fluorescence in the displaced amacrine cells found among RGC cell bodies in the GCL, complicating RGC identification.[9,12,15] However, no overlap was found between tdTomato and amacrine cells labeled with an antibody against choline acetyltransferase (ChAT; Figure 2C and Figure S3).[42–44] This is supported by previous transcriptomic and immunofluorescence analyses, indicating *Slc17a6* was not detectably expressed by any amacrine cell subtypes.[22,45,46]

3.3 | The retina of transgenic mice expressing tdTomato under the Slc17a6 promoter can be used to follow progression in nerve injury models

As the rapid screening of RGC survival after insult is an important application of the *Slc17a6*-tdTomato model, two disease models were used to injure RGCs and evaluate their survival. The optic nerve crush model creates severe injury directly to the optic nerve, with a significant loss of more than 60% of RGCs soma typically detected within a week.[47–50] Fluorescent images from the retinal wholemount of *Slc17a6*-tdTomato mice illustrate the loss of signal 7 days after the nerve crush in the affected eye, as compared to the contralateral eye (Figure 3A). The fluorescent signal enabled a rapid determination of the remaining RGC soma, with quantification indicating a $66.1 \pm 5.3\%$ loss of tdTomato-labeled RGC counts 7 days post-crush (Figure 3B).

The tdTomato fluorescence was also used to track RGC survival in response to the elevation of IOP to 59 mmHg

for 4 h. Images indicate a loss of RGCs 10 days after the elevation of IOP, as expected (Figure 3C).[32] Co-labeling retinal wholemounts with an antibody against BRN3A showed a similar loss. Quantification indicated a parallel level of RGC loss was obtained with both tdTomato-labeled and BRN3A-labeled RGC counts, with a Pearson's correlation of 0.968 between the loss detected with the two signals (Figure 3D).

3.4 | Identification of live RGCs in primary culture of mixed retinal cells from the Slc17a6-tdTomato mice

Cultured neurons provide a powerful tool with which to examine mechanisms of neurite outgrowth and screen for agents that can induce or prevent neurodegeneration. Although neurons grow best in "mixed cultures" containing astrocytes and other cells, identifying a particular cell type from a mixed population of cell types is complex, particularly in live cell experiments that can preclude the use of antibodies. Primary cultures of mixed retinal cells were generated from *Slc17a6*-tdTomato mouse pups to determine whether sufficient fluorescence remained in culture to track neurite growth (Figure 4A).

Initial experiments tracked the growth of RGC neurites (Figure 4B). While the fluorescent signal was strongest from the soma, the signal was sufficiently bright to allow easy detection of neurites. Images were obtained on a standard tissue culture microscope fitted with a color camera; while resolution was not as high as with confocal microscopy, this illustrates the feasibility of using cultured RGCs from the *Slc17a6*-tdTomato mice for rapid screening. The development of neurites was recorded, from the round soma after plating to the emergence of neurites on 3–4 days in vitro (DIV) and the establishment of complex neural interactions by DIV 7. The fluorescent somas were easily tracked, indicating a reduction in the soma number corresponding to the time the neurites emerged (Figure 4C). Overall, these cultures represented a significant advance over our previous attempts to grow RGCs,[51,52] with cells maintained for at least 4 weeks.
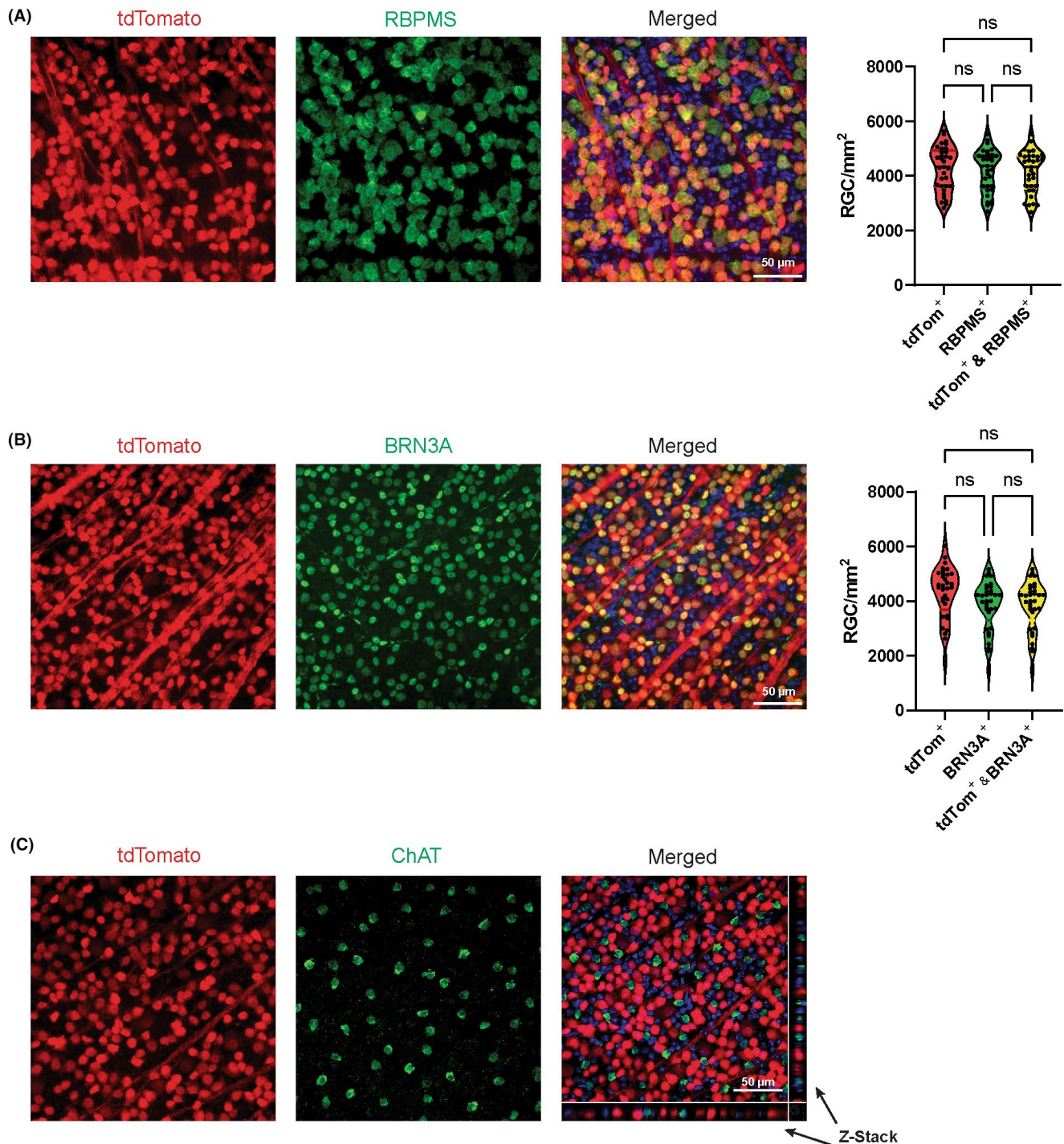
FIGURE 2 *Slc17a6* Cre-driven tdTomato expression labeled >98% of retinal ganglion cells but not amacrine cells. (A) Representative images of retinal wholemounts showing tdTomato (Red) and immunostaining for RBPMS (Green). Overlapping images suggest a high degree of co-localization. On the right, quantitative analysis shows no difference between the number of cells positive for tdTomato, RPBMS or both markers. (One-way ANOVA followed by Tukey post-hoc test; $n = 33$ images; 3 mice per group). Throughout the Figures, bars represent mean $\pm$ SD, and significance is shown as ns >0.05 . (B) Similar images indicating colocalization of tdTomato and cells immunostained for BRN3A (Green) with quantification. (C) ChAT-positive amacrine cells showed no overlap with *Slc17a6* Cre-driven tdTomato expression in wholemount retinal sections.

Imaging of cells using confocal microscopy enabled more precise detection of fine neurite branches (Figure 4D). The complex overlapping of fluorescent neurites was evident. Immunostaining with GFAP indicated astrocytes and/or Müller cells frequently grew in close proximity to the tdTomato-positive RGCs (Figure 4E).
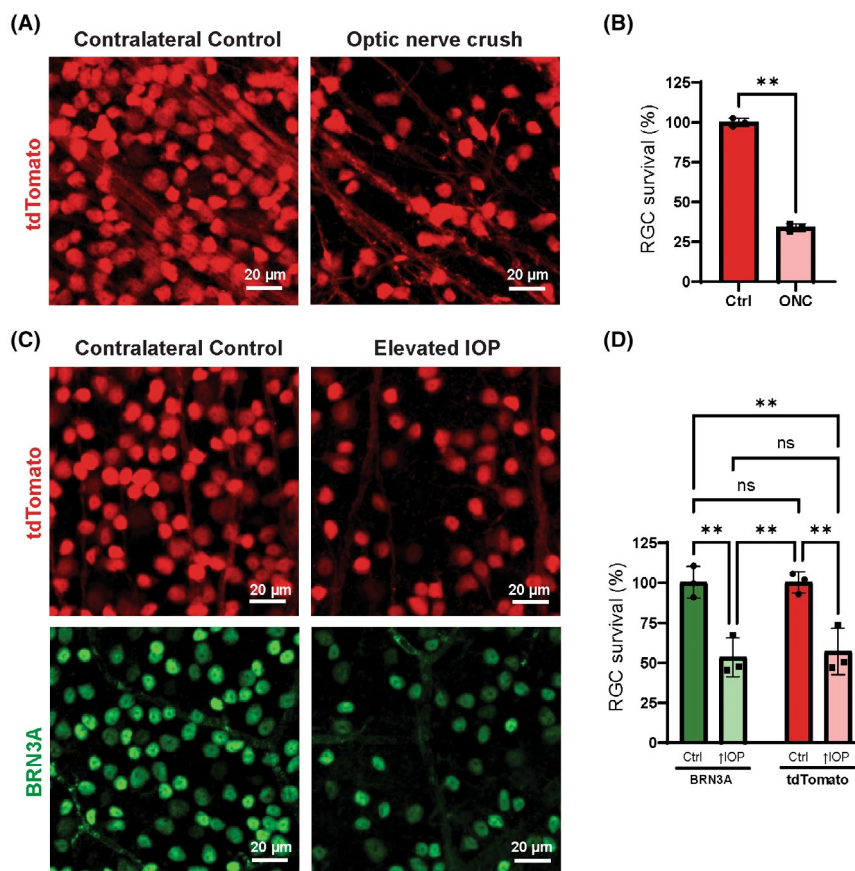
FIGURE 3 tdTomato labeling RGCs under the *Slc17a6* promoter can be used to trace the health of the RGCs. (A) Representative retinal wholemount images from the retinal wholemount of *Slc17a6*-tdTomato mice 7 days after the optic nerve of one eye was crushed (right); the contralateral control eye is shown on the left. (B) Quantification of the RGC soma survival in retinal images of mice 7 days after optic nerve crush. Significant reductions in tdTomato-positive RGC soma were observed in the crushed eye compared to the control eye after 7 days. (Paired *t*-test; $n=3$). (C) Representative retinal wholemount images from Slc7A6-tdTomato mice 10 days after a transient elevation of IOP showing a decrease in tdTomato fluorescence (top) and BRN3A immunofluorescence (bottom) from the same retinal wholemount. (D) Comparable reduction in the number of BRN3A and tdTomato-positive cells quantified 10 days after IOP elevation. (Two-way ANOVA followed by Tukey post-hoc test; ** $p<0.01$; $n=3$; bars represent mean $\pm$ SD throughout).

The measurement of intracellular Ca^{2+} enables the physiological responses of RGCs to be better understood on a more mechanistic level. While the bright fluorescent signal facilitated the identification of RGCs in mixed retinal cultures, standard assays to determine intracellular Ca^{2+} also depend on fluorescent readouts. To determine whether the *Slc17a6*-tdTomato mice could be used for Ca^{2+} measurements, the ratiometric Ca^{2+} reporter Fura-2 was selected as its excitation wavelengths of 340 and 380 nm are far removed from the td-Tomato excitation of 554 nm. The red fluorescence was used to guide the selection of the "Region of Interest" from the mixed cultures. Adding P2X7R agonist BzATP evoked rapid, reversible, and repeatable responses in the RGCs similar to those recorded from wild-type RGCs (Figure 4F).[53] This suggests that RGCs obtained from *Slc17a6*-tdTomato mice in neuronal culture can be used for Ca^{2+} measurements, at least using the Fura-2 Ca^{2+}

reporter. For example, preliminary data suggest the cells can help compare the response to Piezo channel activation in soma and neurites.[54]

3.5 | Slc17a6 Cre-driven tdTomato labeling of RGCs does not interfere with RGC function or retinal structure

To determine whether the expression of tdTomato fluorochrome led to any gross changes in retinal function or RGC output, microelectrode array (MEA) recordings were performed using retinal wholemounts from *Slc17a6*-tdTomato mice and controls. No differences were observed in the responses to 2 s flashes of 455 nm light (Figure 5A). The firing rate of the transient ON-response across a range of intensities was determined to compare the responses quantitatively. No significant change was
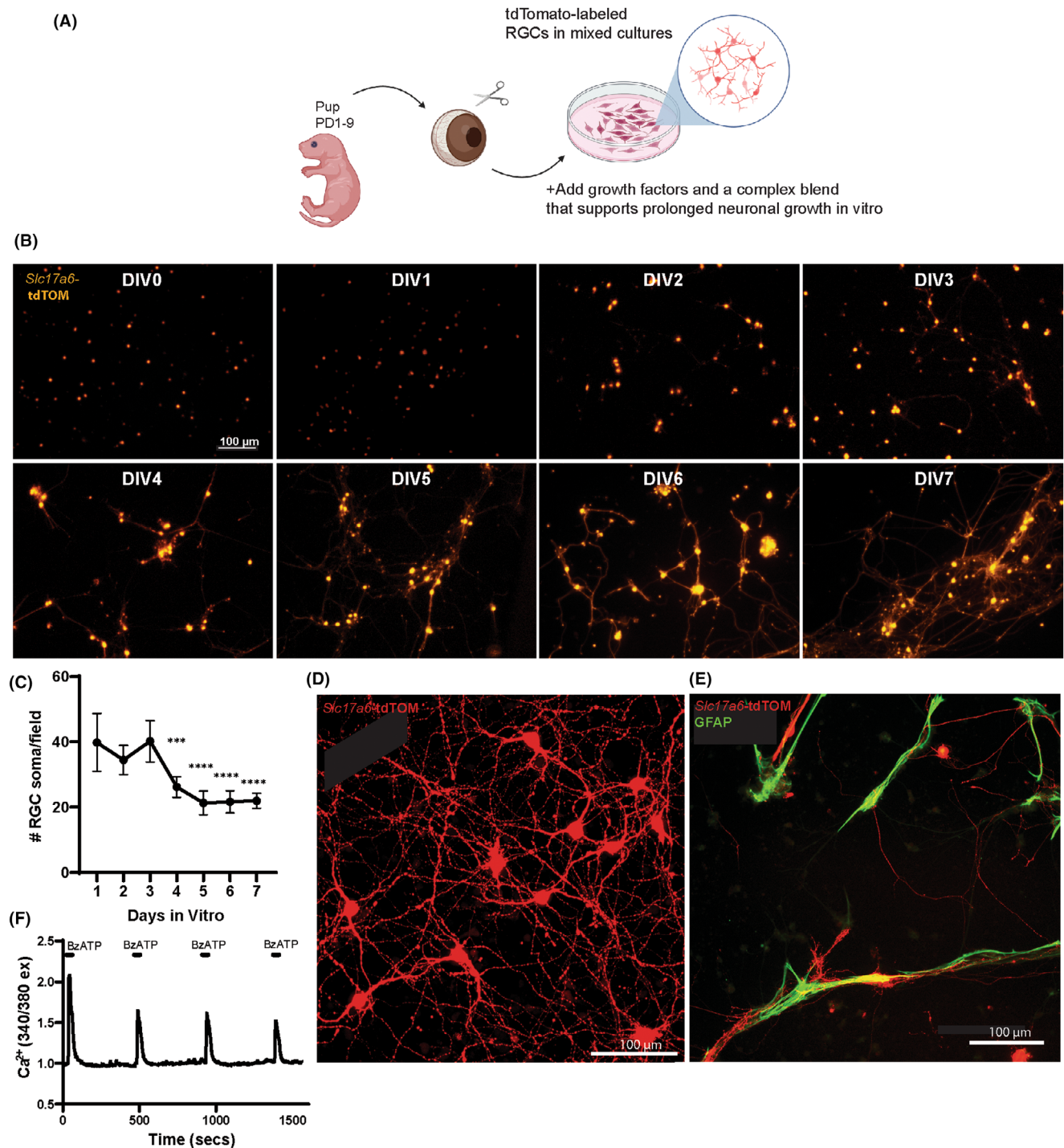
FIGURE 4 RGC identification in primary cultures of mixed retinal cells from *Slc17a6*-tdTomato mice. (A) Schematic showing culture procedure for examining fluorescent cells in a mixed retinal culture. (B) Representative images of live cells from a tissue culture microscope showing the growth of fluorescent neurites over 7 days in vitro (DIV). (C) Counts of fluorescent soma indicate a reduction after 3 DIV, corresponding to the time when the neurites begin to extend (Mean ± SD from 6 coverslips per day). (D) Representative image of tdTomato-labeled RGCs from mixed retinal cultures fixed at 6 DIV and imaged with confocal microscopy. Multiple long neurite processes can be seen extending from the soma. (E) Mixed retinal cultures immunostained for GFAP (green) suggest a close association between growing RGCs and astrocytes and/or Müller cells. (F) Representative of a normalized Fura-2 Ca^{2+} trace of primary mouse tdTomato-labeled RGC in response to 100 μM BzATP. The ratio of light excited at 340–380 nm provides a robust index of Ca^{2+} levels from the mice as normalized to $t = 0$.

detected, suggesting the fluorochrome does not interfere with the function of the RGCs, at least when the retina is stimulated at 455 nm (Figure 5B).

To determine if the expression of the tdTomato fluorochrome induced any gross structural alteration in the retina, optical coherence tomography (OCT) was performed. OCT images were acquired at the center of the optic nerve, and retinal thickness was determined from the nerve fiber layer border to Bruch's membrane. No difference in retinal thickness was detected (Figure 6A,B).

## 3.6 | Visualization and quantification of the Slc17a6- tdTomato signal in vivo

The application of in vivo ocular imaging is a powerful approach that can advance the understanding and treatment of vision-related diseases. Non-invasive cSLO imaging was performed on the *Slc17a6*-tdTomato determine if the mice could be used with in vivo imaging. Initial images showed that nerve fiber bundles could be clearly detected radiating out from the optic nerve head, with a fluorescence readout from the somas suggested further out (Figure 7A,B). While this preponderance of fluorescence was an advantage in some applications, it did complicate quantification in vivo, and resolution

was at its limits. Machine learning was thus used to identify fluorescent soma, with Ilastic trained to distinguish between background and RGC soma (Figure 7B, right). Automatic counting of RGCs in the 51° Field of View (FOV) image spanning across the optic nerve head gave 2994.2 ± 291.9 RGCs/mm^2, while counts performed on a 10° FOV $\sim 400\,\mu m$ from the optic nerve head with fewer axons visible led to 3561.7 ± 426.4 RGCs/mm^2 (Figure 7C). This later value was within 20% of those obtained from manual counting of RGCs in retinal wholemounts images with confocal microscopy above, suggesting the approach had some value. Expanded use of machine learning in the future is expected to improve the robustness of the approach. Finally, fluorescent retinal images obtained with the Micron3 system indicated a similar pattern, with bright fluorescence from the axon bundles radiating out from the optic nerve head and a background signal consistent with somal fluorescence (Figure 7D).

4 | DISCUSSION

The present study characterizes the *Slc17a6*-tdTomato mouse line as a tool to aid in the study of RGCs. Immunostaining with two different RGC markers suggests the td-Tomatofluorescence labels ~all RGCs, but not

FIGURE 5 MEA analysis showed no effect of tdTomato on light-evoked RGC activity. (A) Representative MEA recording at 565,000 photons/s/μm^{-2} depicted comparable light-evoked RGC firing responses between wild-type and *Slc17a6*-tdTomato mice; light flashes were 2 s and 455 nm. (B) No statistical difference was detected in the mean responses across different light intensities between wild-type and tdTomato-labeled RGC mice. (Repeated measures two-way ANOVA tests followed by Sidak post-hoc test; wild-type $n = 19$ retinas; tdTomato-labeled RGC $n = 6$ retinas). Error bars represent mean $\pm$ SD.
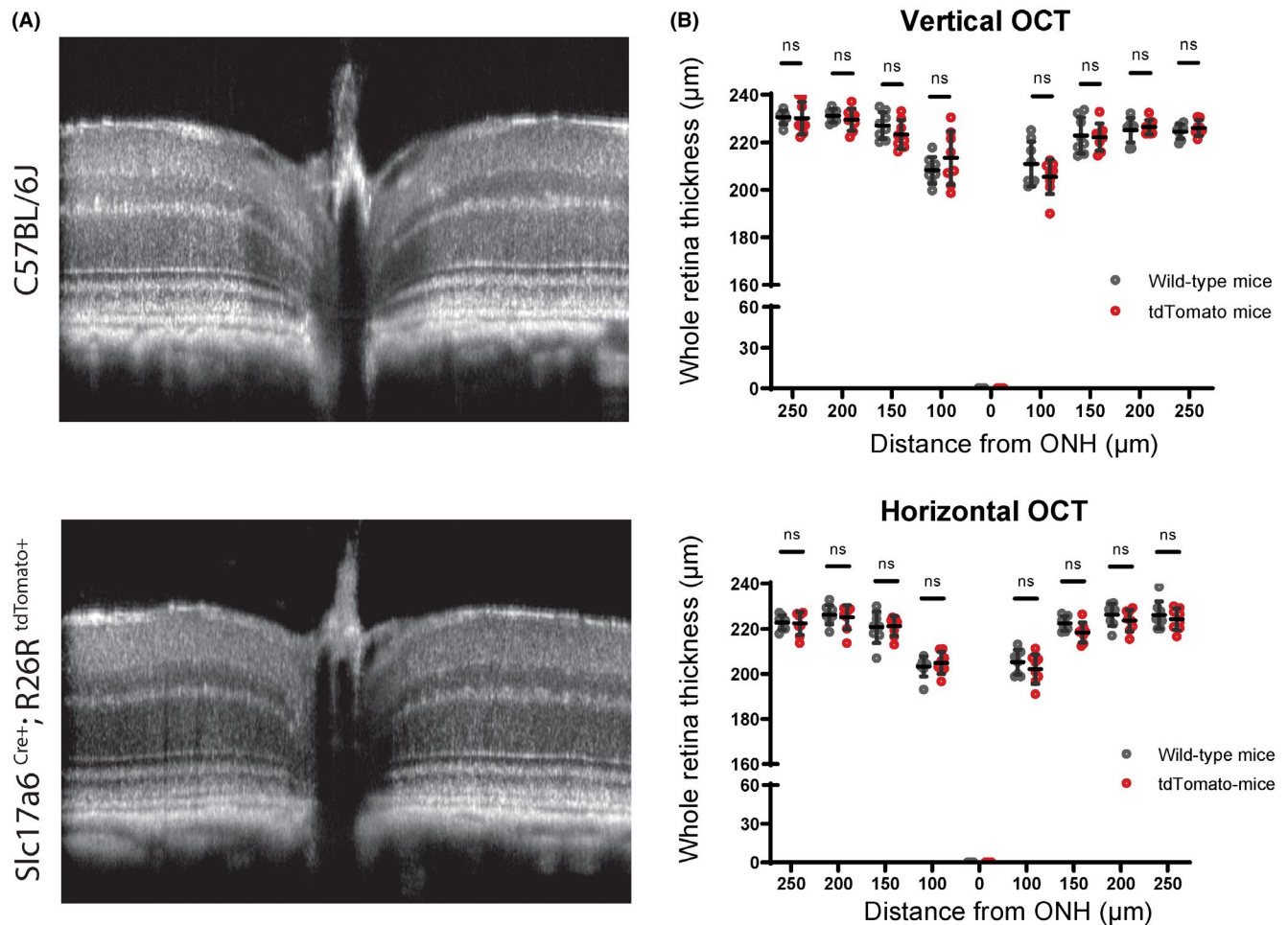
(A)

(B)
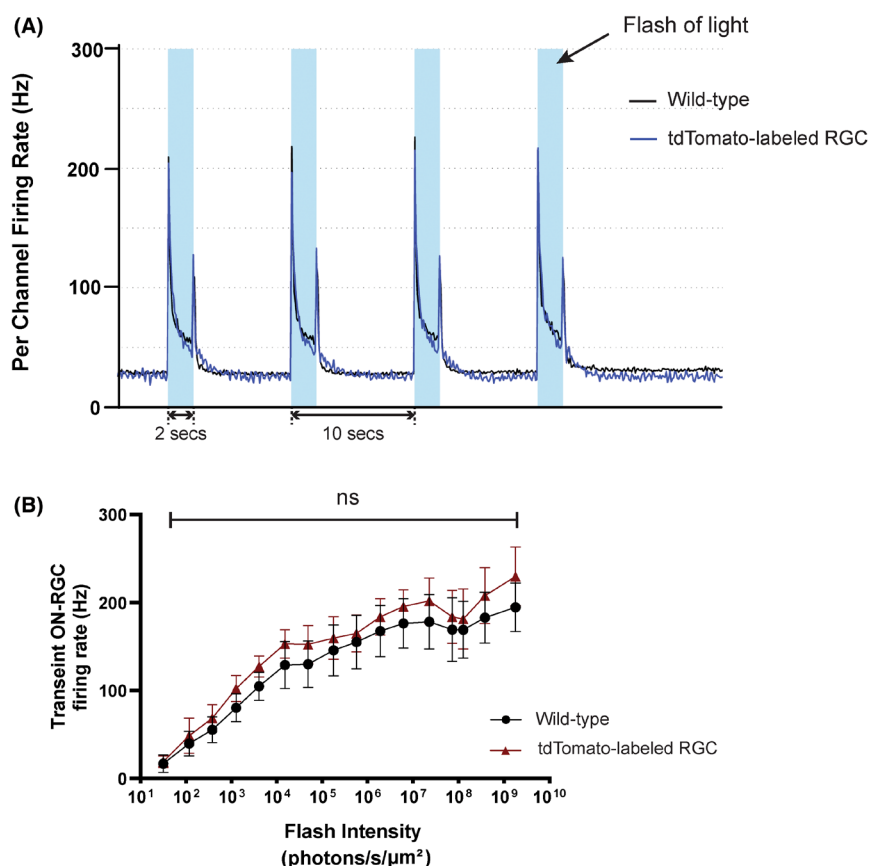
FIGURE 6 Optical coherence tomography (OCT) demonstrated normal retinal architecture and thickness in the *Slc17a6*-tdTomato mice. (A) Representative OCT images from a C57BL/6J mouse (top) compared to a Slc17a6-tdTomato-labeled mouse (bottom). (B) Spider diagrams indicating no difference in retinal thickness of wild-type and Slc17a6-tdTomato mice. (Two-way ANOVA tests followed by Tukey's post-hoc test; $n = 8$ eyes; 4 mice per group; bars represent mean $\pm$ SD throughout).

CHaT-positive displaced amacrine cells. The intensity of the tdTomato fluorescence enabled the detection of RGC dendrites in the IPL in considerable detail when examined with 2-photon microscopy, while expression in the axons extended through the optic nerve head and along the optic nerve. The red signal greatly facilitated the non-invasive daily monitoring of RGC growth in mixed retinal cultures. While the red fluorescence was intense, it did not prevent the readout of intracellular Ca^{2+} when the reporter Fura-2 was employed. The presence of the tdTomato fluorophore in RGCs did not alter spike generation in response to 455 nm light flashes, or alter retinal thickness as measured with OCT. Although the presence of bright axonal fluorescence and dense expression in ~all RGCs somewhat complicated detection of individual cells in vivo, quantification was possible using machine learning to detect somal patterns. Overall, the *Slc17a6*-tdTomato reporter mouse is a powerful tool to simplify the analysis of RGCs.

4.1 | Specificity and selectivity of fluorescence in Slc17a6-tdTomato mouse

The ideal reporter will fluoresce in all RGCs and only in RGCs. With regards to the first concern, >98% of the cells positive for RBPMS in the *Slc17a6*-tdTomato mouse also emitted a red fluorescence. RBPMS expression was previously reported in all cells positively immunostained for melanopsin, BRN3A, and SMI-32, suggesting it identified ~all RGCs.[39] This agrees with the RNAseq analysis showing *Slc17a6* expressed in all 45 molecularly distinct RGC types in adult mice,[18] and fluorescent analysis of a *Slc17a6*-Cre reporter mouse.[21] Furthermore, 100% of cells positive for BRN3A were also positive for tdTomato, while 89% of the fluorescent cells in the RGC layer were also positive for BRN3A; this is very close to the proportion of RBPMS cells positive for BRN3A.[39] The signal intensity did vary between cells; this could reflect differences in the activity of the *Slc17a6* promotor

FIGURE 7 In vivo visualization of the fluorescence in *Slc17a6*- tdTomato mice. (A) cSLO detected fluorescence in transgenic mice (right) but not from wild-type retina (left) both 102° Field of View (FOV). (B) Bright fluorescence from axon bundles in the nerve fiber layer and a somewhat punctate signal was detected at a 51° FOV. The Ilastic machine learning algorithm was trained to recognize background (green) and RGC soma (red) using 10° FOV images (right) and 51° FOV images. The red insert indicates the location of the 10° FOV region. (C) Comparison of RGC counts obtained using Ilastic-trained measurements from 51° FOV images 10° FOV images and from manual counts from ex vivo retinal wholemounts. Dots represent six eyes from 3 Slc17a6-tdTomato mice for the in vivo counts, and counts from the wholemounts used for both BRN3B and RPBMS studies in Figure 2; bars represent mean ± SD throughout. **$p = 0.0012$. (D) Representative image of a Slc17a6-tdTomato mouse obtained using a Micron3 system.
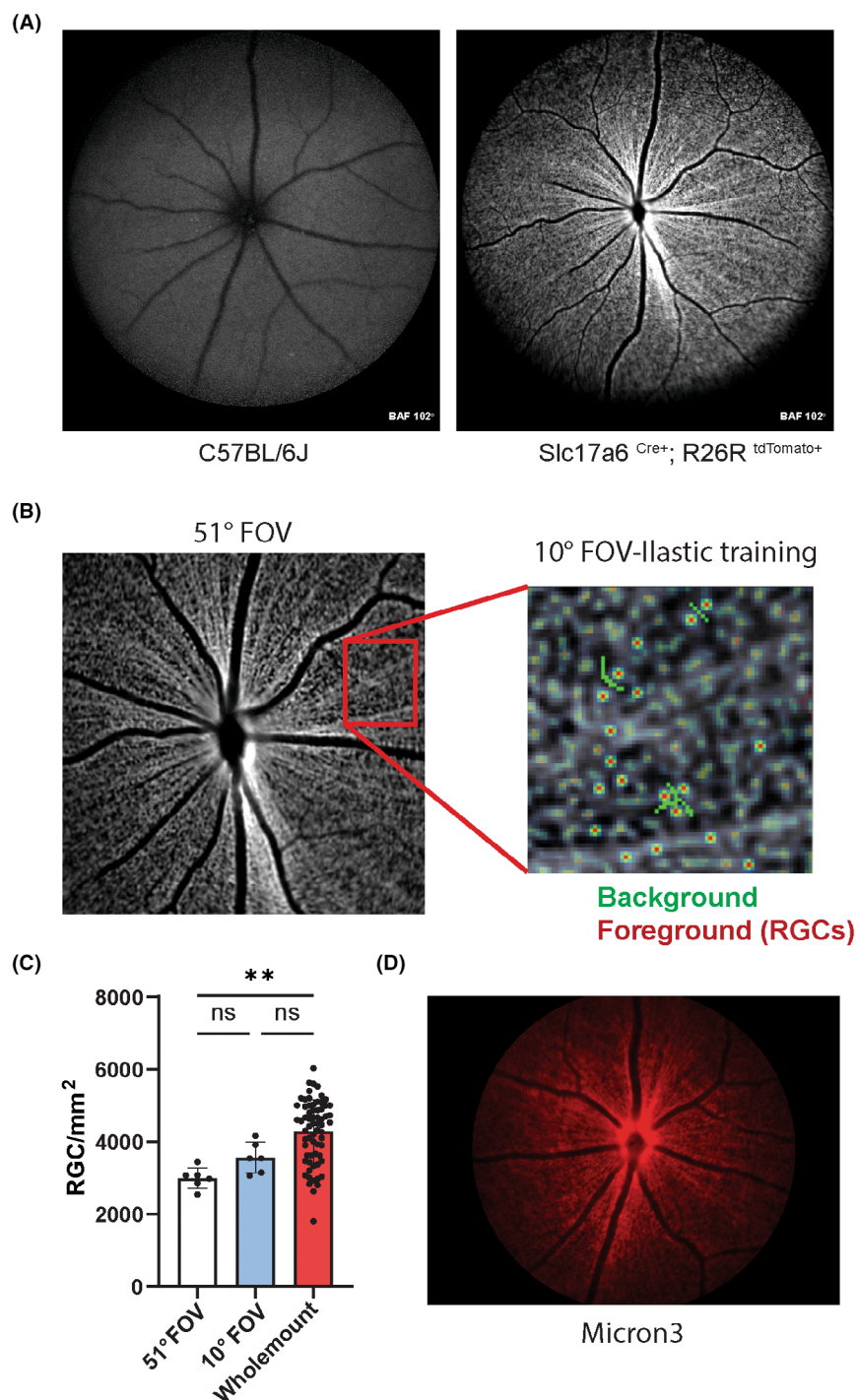
in different RGC types, as previously reported, although differential expression of *Slc17a6* was not found between ON-, OFF- and ON/OFF RGCs.[18,20] Regardless, the signal was always bright enough to enable the detection of fluorescence in all RBPMS-positive cells. Together, this implies that close to all of the RGCs are labeled in the *Slc17a6*-tdTomato mouse.

   Slc17a6 codes for vesicular glutamate transporter 2 (*Vglut2*), and *VGlut2* is extensively distributed in mouse, macaque, and human visual cortex in addition to other brain regions and somatic nerves.[55,56] TdTomato expression

is predicted to be observed in these areas as well, although this awaits confirmation for the mice used in the present study. This neural expression means crossing the *Slc17a6* Cre mice with mice floxed for critical genes runs the risk of systemic and/or developmental issues (as we discovered attempting to knockout Piezo channels in RGCs with the *Slc17a6* promotor). However, the more limited expression of *Slc17a6* in the retina makes tdTomato reporter relatively specific for RGCs within the inner retina. While a proportion of horizontal cells were also fluorescent within the retina, and expression in a select proportion of cones

has been reported,[22] spatial segregation across retail layers should aid in selective detection of RGC.

4.2 | Fluorescence in dendrites, soma, and axons

The intense labeling of the RGCs soma in the *Slc17a6*-tdTomato mice facilitates quantification of RGCs; the mouse enables a rapid count of surviving RGCs from the wholemount after insults such as optic nerve crush, without the time and expense of immunolabeling. The ability to detect detailed projection of dendrites into the INL may help assess the degree of dendritic retraction associated with glaucoma, for example.[57] The intense fluorescence from axons in the optic nerve head and myelinated portions of the optic nerve beyond the globe should facilitate analysis of their role in visual processing and disease, particularly as other RGC markers can show a preference for staining the soma.

Our initial analysis suggests the robust endogenous expression of tdTomato may also enable visualization of RGCs in an in vivo setting, although certain adaptations may be necessary as the presence of fluorescence in axon bundles, dendrites, and ~all RGC soma can actually interfere with soma counting. The use of machine learning processes such as Ilastic to train the automated counts to ignore the axon bundles improved the accuracy of RGC counts in our hands. The reduced RGC numbers obtained when the 51° FOV was assessed as compared to a smaller region away from the optic nerve head (2994.2 ± 291.9 vs. 3561.7 ± 426.4 RGCs/mm^2, respectively) likely reflect regions taken up by blood vessels and axon bundles not available for counting. The RGC density tabulated in vivo was within 20% of the density determined with manual counts from the wholemount; considering the field size was calibrated by assuming the optic disc was 0.225 mm in diameter, this is reasonable.[36] Further validation of the machine learning approach is needed before using the in vivo cSLO images for more than a screening approach, however.

The application of tdTomato-labeled RGCs in cell culture also demonstrated potential for monitoring the effects of molecular manipulation on neurite outgrowth and health of the RGCs. Neuronal/glial interactions can be examined in mixed cultures, although the presence of a genetically driven fluorophore aids in neural detection.[58] The ability to detect neurite growth without fixation may improve a temporal understanding of the processes, or at least make it less expensive. Immunostaining the mixed retinal cultures generated from *Slc17a6*-tdTomato mice for GFAP could suggest a close intertwining of Müller cells or astrocytes and

elongations of RGC neurites (Figure 4E); this may have implications for recent work suggesting markers for the neurotoxic A1 astrocyte state rise following stimulation of the P2X7 receptor for ATP.[59] Some tdTomato-labeled horizontal cells and cones are expected in the mixed culture from SLC17a6-tdTomato mice; this should be minimal, however, given the low percentage of positive labeling detected within their total population.[22,40,60] The complex neurite branching seen here is also more consistent with RGC growth, although this needs to be confirmed empirically.

4.3 | Advantages, controls, and limitations of the Slc17a6-tdTomato mouse

RGCs represent a heterogeneous population of neurons that can be segregated into more than 40 subtypes based on their morphological, physiological, gene expression, and mosaic characteristics,[18,61,62] thereby hindering the development of a pan-RGC reporter line. A recent comprehensive screening of 88 Cre transgenic driver lines suggests the *Slc17a6*-Cre line demonstrates good specificity for targeting a broad range of RGC subtypes.[21] In the present study, we demonstrated the effectiveness and specificity of the *Slc17a6*-Cre line in labeling RGC by cross-breeding with Cre reporter Ai9 mice, as well as explored its potential as a valuable tool for RGC research. Previous RGC reporter transgenic mice showed non-specific labeling of amacrine and Müller cells.[9,12] As the results above suggest the *Slc17a6*-tdTomato mouse shows a signal in >98% of the RGCs without labeling other cell types in the GCL, this mouse provides several advantages for more precise studies of RGCs.

While the present study emphasized many potential benefits of the *Slc17a6*-tdTomato mouse, controls implied that the presence of an intense red fluorescence in RGCs is not itself detrimental. OCT analysis indicated retinal thickness was not altered in the *Slc17a6*-tdTomato mouse; as retinal thickness can be altered with swelling, inflammatory response, or cell loss, the absence of a change suggests the presence of tdTomato is benign. The overall retinal output, defined as the frequency of action potentials generated by RGCs detected with an MEA, was the same in wild-type and *Slc17a6*-tdTomato mice, suggesting the response to light flashes was not affected by the presence of the fluorophore. Of course this could be affected by the wavelength of light used; the light flashes in our MEA system were 455 nm; whether the response to a red-shifted light is affected remains to be determined. However, the results above indicate the presence of the fluorophore itself does not impact the overall signaling processes.

5 | CONCLUSION

The above characterization of the *Slc17a6*-tdTomato mouse suggests it presents a fluorescent signal in ~all RGCs types while also showing specificity within the inner retina. The bright signal in RGC dendrites, in axons through the optic nerve head and myelinated nerve may help studies of axonal degeneration and dendritic retraction. The mouse can facilitate screening of RGC survival in retinal wholemounts, while in vivo quantification may be possible with certain adaptations; future improvements to imaging and machine learning should enable better in vivo monitoring. The successful integration of this reporter into transgenic mouse models without altering the physiological integrity of RGCs confirms its utility and reliability for continuous, longitudinal studies. Applying this RGC reporter in diverse research settings promises to broaden our understanding of RGC dynamics under various pathological conditions, leading to more targeted and effective therapeutic strategies.

AUTHOR CONTRIBUTIONS

P.S. made substantial contributions to the conception and design of the work, the acquisition, analysis, and interpretation of data, and drafted and edited the work; W.L. made substantial contributions to the conception and design of the work, the acquisition, analysis, and interpretation of data; S.N. made substantial contributions to acquisition, analysis, and interpretation of data; S.P. made substantial contributions to the analysis of data; S.H. made substantial contributions to the analysis of data; T.Y. made substantial contributions to the acquisition of data; Q.C. helped edit the work; B.A.B. made substantial contributions to the acquisition and analysis of data; C.H.M made substantial contributions to the conception and design of the work, analysis, and interpretation of data, and drafted and edited the work. All authors have approved the submitted version and agreed both to be personally accountable for the author's own contributions and to ensure that questions related to the accuracy or integrity of any part of the work are appropriately investigated, resolved, and the resolution documented in the literature.

CONFLICT OF INTEREST STATEMENT

All the authors have read the manuscript and declare no conflict of interest.

ORCID

Puttipong Sripinun https://orcid.org/0009-0001-1717-9962
Sergei Nikonov https://orcid.org/0000-0001-7212-1272
Tianyuan Yao https://orcid.org/0000-0002-8301-7144
Brent A. Bell https://orcid.org/0000-0003-2827-1892
Claire H. Mitchell https://orcid.org/0000-0002-9784-6672

REFERENCES

1. Sernagor E, Eglen SJ, Wong RO. Development of retinal ganglion cell structure and function. *Prog Retin Eye Res*. 2001;20:139-174.
2. Laha B, Stafford BK, Huberman AD. Regenerating optic pathways from the eye to the brain. *Science*. 2017;356:1031-1034.
3. Levin LA, Louhab A. Apoptosis of retinal ganglion cells in anterior ischemic optic neuropathy. *Arch Ophthalmol*. 1996;114:488-491.
4. Kern TS, Barber AJ. Retinal ganglion cells in diabetes. *J Physiol*. 2008;586:4401-4408.
5. Almasieh M, Wilson AM, Morquette B, Vargas JLC, Di Polo A. The molecular basis of retinal ganglion cell death in glaucoma. *Prog Retin Eye Res*. 2012;31:152-181.
6. You Y, Gupta VK, Li JC, Klistorner A, Graham SL. Optic neuropathies: characteristic features and mechanisms of retinal ganglion cell loss. *Rev Neurosci*. 2013;24:301-321.
7. Smith C, Vianna J, Chauhan B. Assessing retinal ganglion cell damage. *Eye*. 2017;31:209-217.
8. Corral-Domenge C, de la Villa P, Mansilla A, Germain F. Tools and biomarkers for the study of retinal ganglion cell degeneration. *Int J Mol Sci*. 2022;23:4287.
9. Feng G, Mellor RH, Bernstein M, et al. Imaging neuronal subsets in transgenic mice expressing multiple spectral variants of GFP. *Neuron*. 2000;28:41-51.
10. Leung CK-s, Weinreb RN, Li ZW, et al. Long-term in vivo imaging and measurement of dendritic shrinkage of retinal ganglion cells. *Invest Ophthalmol Vis Sci*. 2011;52:1539-1547.
11. Oglesby E, Quigley HA, Zack DJ, et al. Semi-automated, quantitative analysis of retinal ganglion cell morphology in mice selectively expressing yellow fluorescent protein. *Exp Eye Res*. 2012;96:107-115.
12. Raymond ID, Vila A, Huynh U-CN, Brecha NC. Cyan fluorescent protein expression in ganglion and amacrine cells in a thy1-CFP transgenic mouse retina. *Mol Vis*. 2008;14:1559.
13. Wang X, Archibald ML, Stevens K, Baldridge WH, Chauhan BC. Cyan fluorescent protein (CFP) expressing cells in the retina of Thy1-CFP transgenic mice before and after optic nerve injury. *Neurosci Lett*. 2010;468:110-114.
14. Leung CK, Lindsey JD, Crowston JG, et al. In vivo imaging of murine retinal ganglion cells. *J Neurosci Methods*. 2008;168:475-478.

15. Walsh MK, Quigley HA. In vivo time-lapse fluorescence imaging of individual retinal ganglion cells in mice. *J Neurosci Methods*. 2008;169:214-221.

16. Miltner AM, Mercado-Ayon Y, Cheema SK, Zhang P, Zawadzki RJ, La Torre A. A novel reporter mouse uncovers endogenous Brn3b expression. *Int J Mol Sci*. 2019;20:2903.

17. Li G, Luo Y, Zhang Q, et al. The RBPMS(CreERT2-tdTomato) mouse line for studying retinal and vascular relevant diseases. *iScience*. 2023;26:108111.

18. Tran NM, Shekhar K, Whitney IE, et al. Single-cell profiles of retinal ganglion cells differing in resilience to injury reveal neuroprotective genes. *Neuron*. 2019;104:1039-1055.e1012.

19. Stella SL Jr, Li S, Sabatini A, Vila A, Brecha NC. Comparison of the ontogeny of the vesicular glutamate transporter 3 (VGLUT3) with VGLUT1 and VGLUT2 in the rat retina. *Brain Res*. 2008;1215:20-29.

20. Huang W, Xu Q, Su J, et al. Linking transcriptomes with morphological and functional phenotypes in mammalian retinal ganglion cells. *Cell Rep*. 2022;40:111322.

21. Martersteck EM, Hirokawa KE, Evarts M, et al. Diverse central projection patterns of retinal ganglion cells. *Cell Rep*. 2017;18:2058-2072.

22. Wang L, Klingeborn M, Travis AM, Hao Y, Arshavsky VY, Gospe SM III. Progressive optic atrophy in a retinal ganglion cell-specific mouse model of complex I deficiency. *Sci Rep*. 2020;10:16326.

23. Albalawi F, Lu W, Beckel JM, Lim JC, McCaughey SA, Mitchell CH. The P2X7 receptor primes IL-1β and the NLRP3 inflammasome in astrocytes exposed to mechanical strain. *Front Cell Neurosci*. 2017;11:227.

24. Kalesnykas G, Oglesby EN, Zack DJ, et al. Retinal ganglion cell morphology after optic nerve crush and experimental glaucoma. *Invest Ophthalmol Vis Sci*. 2012;53:3847-3857.

25. Morrison JC, Cepurna WO, Tehrani S, et al. A period of controlled elevation of IOP (CEI) produces the specific gene expression responses and focal injury pattern of experimental rat glaucoma. *Invest Ophthalmol Vis Sci*. 2016;57:6700-6711.

26. Crowston JG, Kong YX, Trounce IA, et al. An acute intraocular pressure challenge to assess retinal ganglion cell injury and recovery in the mouse. *Exp Eye Res*. 2015;141:3-8.

27. Lim JC, Lu W, Beckel JM, Mitchell CH. Neuronal release of cytokine IL-3 triggered by mechanosensitive autostimulation of the P2X7 receptor is neuroprotective. *Front Cell Neurosci*. 2016;10:270.

28. Campagno KE, Lu W, Jassim AH, et al. Rapid morphologic changes to microglial cells and upregulation of mixed microglial activation state markers induced by P2X7 receptor stimulation and increased intraocular pressure. *J Neuroinflammation*. 2021;18:217.

29. Winzeler A, Wang JT. Purification and culture of retinal ganglion cells from rodents. *Cold Spring Harb Protoc*. 2013;2013:643.

30. Chen Y, Stevens B, Chang J, Milbrandt J, Barres BA, Hell JW. NS21: re-defined and modified supplement B27 for neuronal cultures. *J Neurosci Methods*. 2008;171:239-247.

31. Gómez NM, Lu W, Lim J, et al. Robust lysosomal calcium signaling through channel TRPML1 is impaired by lipofuscin accumulation. *FASEB J*. 2018;32:782-794.

32. Lu W, Albalawi F, Beckel JM, Lim JC, Laties AM, Mitchell CH. The P2X7 receptor links mechanical strain to cytokine IL-6 up-regulation and release in neurons and astrocytes. *J Neurochem*. 2017;141:436-448.

33. Mitchell CH, Lu W, Hu H, Zhang X, Reigada D, Zhang M. The P2X(7) receptor in retinal ganglion cells: a neuronal model of pressure-induced damage and protection by a shifting purinergic balance. *Purinergic Signal*. 2009;5:241-249.

34. Anderson BD, Lee T, Bell B, Song Y, Dunaief JL. Low ceruloplasmin levels exacerbate retinal degeneration in a hereditary hemochromatosis model. *Dis Model Mech*. 2023;16:dmm050226.

35. Berg S, Kutra D, Kroeger T, et al. Ilastik: interactive machine learning for (bio)image analysis. *Nat Methods*. 2019;16:1226-1232.

36. Paques M, Simonutti M, Roux MJ, et al. High resolution fundus imaging by confocal scanning laser ophthalmoscopy in the mouse. *Vis Res*. 2006;46:1336-1345.

37. Gaub BM, Berry MH, Holt AE, et al. Restoration of visual function by expression of a light-gated mammalian ion channel in retinal ganglion cells or ON-bipolar cells. *Proc Natl Acad Sci*. 2014;111:E5574-E5583.

38. Sharma RK, Netland PA. Early born lineage of retinal neurons express class III β-tubulin isotype. *Brain Res*. 2007;1176:11-17.

39. Rodriguez AR, de Sevilla Müller LP, Brecha NC. The RNA binding protein RBPMS is a selective marker of ganglion cells in the mammalian retina. *J Comp Neurol*. 2014;522:1411-1443.

40. Gong J, Jellali A, Mutterer J, Sahel JA, Rendon A, Picaud S. Distribution of vesicular glutamate transporters in rat and human retina. *Brain Res*. 2006;1082:73-85.

41. Nadal-Nicolás FM, Jiménez-López M, Sobrado-Calvo P, et al. Brn3a as a marker of retinal ganglion cells: qualitative and quantitative time course studies in naive and optic nerve–injured retinas. *Invest Ophthalmol Vis Sci*. 2009;50:3860-3868.

42. Haverkamp S, Wässle H. Immunocytochemical analysis of the mouse retina. *J Comp Neurol*. 2000;424:1-23.

43. Zhang J, Yang Z, Wu SM. Development of cholinergic amacrine cells is visual activity-dependent in the postnatal mouse retina. *J Comp Neurol*. 2005;484:331-343.

44. Zhang C, Yu WQ, Hoshino A, et al. Development of ON and OFF cholinergic amacrine cells in the human fetal retina. *J Comp Neurol*. 2019;527:174-186.

45. Filippi A, Mueller T, Driever W. vglut2 and gad expression reveal distinct patterns of dual GABAergic versus glutamatergic cotransmitter phenotypes of dopaminergic and noradrenergic neurons in the zebrafish brain. *J Comp Neurol*. 2014;522:2019-2037.

46. Jo A, Xu J, Deniz S, Cherian S, DeVries SH, Zhu Y. Intersectional strategies for targeting amacrine and ganglion cell types in the mouse retina. *Front Neural Circuits*. 2018;12:66.

47. Berkelaar M, Clarke D, Wang Y, Bray G, Aguayo A. Axotomy results in delayed death and apoptosis of retinal ganglion cells in adult rats. *J Neurosci*. 1994;14:4368-4374.

48. Levkovitch-Verbin H, Harris-Cerruti C, Groner Y, Wheeler LA, Schwartz M, Yoles E. RGC death in mice after optic nerve crush injury: oxidative stress and neuroprotection. *Invest Ophthalmol Vis Sci*. 2000;41:4169-4174.

49. Sánchez-Migallón MC, Valiente-Soriano FJ, Nadal-Nicolás FM, Vidal-Sanz M, Agudo-Barriuso M. Apoptotic retinal ganglion cell death after optic nerve transection or crush in mice: delayed RGC loss with BDNF or a caspase 3 inhibitor. *Invest Ophthalmol Vis Sci*. 2016;57:81-93.

50. Li L, Huang H, Fang F, Liu L, Sun Y, Hu Y. Longitudinal morphological and functional assessment of RGC neurodegeneration after optic nerve crush in mouse. *Front Cell Neurosci.* 2020;14:109.

51. Zhang M, Hu H, Zhang X, et al. The A3 adenosine receptor attenuates the calcium rise triggered by NMDA receptors in retinal ganglion cells. *Neurochem Int.* 2010;56:35-41.

52. Xia J, Lim JC, Lu W, et al. Neurons respond directly to mechanical deformation with pannexin-mediated ATP release and autostimulation of P2X7 receptors. *J Physiol.* 2012;590:2285-2304.

53. Zhang X, Zhang M, Laties AM, Mitchell CH. Stimulation of P2X7 receptors elevates Ca^{2+} and kills retinal ganglion cells. *Invest Ophthalmol Vis Sci.* 2005;46:2183-2191.

54. Sripinun P, See LP, Nikonov S, et al. Piezo1 and Piezo2 channels in retinal ganglion cells and the impact of Piezo1 stimulation on light-dependent neural activity. *BIORXIV.* 2024;599589. doi:10.1101/2024.06.25.599602

55. Coleman JE, Nahmani M, Gavornik JP, et al. Rapid structural remodeling of thalamocortical synapses parallels experience-dependent functional plasticity in mouse primary visual cortex. *J Neurosci.* 2010;30:9670-9682.

56. Garcia-Marin V, Ahmed TH, Afzal YC, Hawken MJ. Distribution of vesicular glutamate transporter 2 (VGluT2) in the primary visual cortex of the macaque and human. *J Comp Neurol.* 2013;521:130-151.

57. Tribble JR, Vasalauskaite A, Redmond T, et al. Midget retinal ganglion cell dendritic and mitochondrial degeneration is an early feature of human glaucoma. *Brain Commun.* 2019;1:fcz035.

58. Guttenplan KA, Liddelow SA. Astrocytes and microglia: models and tools. *J Exp Med.* 2019;216:71-83.

59. Campagno KE, Sripinun P, See LP, et al. Increased pan-type, A1-type, and A2-type astrocyte activation and upstream inflammatory markers are induced by the P2X7 receptor. *Int J Mol Sci.* 2024;25:8784.

60. Wässle H, Regus-Leidig H, Haverkamp S. Expression of the vesicular glutamate transporter vGluT2 in a subset of cones of the mouse retina. *J Comp Neurol.* 2006;496:544-555.

61. Sanes JR, Masland RH. The types of retinal ganglion cells: current status and implications for neuronal classification. *Annu Rev Neurosci.* 2015;38:221-246.

62. Rheaume BA, Jereen A, Bolisetty M, et al. Single cell transcriptome profiling of retinal ganglion cells identifies cellular subtypes. *Nat Commun.* 2018;9:2759.

63. Sripinun P, Lu W, Nikonov S, et al. Slc17a6 Cre-driven tdTomato transgenic mice as a tool for studying retinal ganglion cells. *Biorxiv.* 2024;06.20.599589. doi:10.1101/2024.06.20.599589

SUPPORTING INFORMATION

Additional supporting information can be found online in the Supporting Information section at the end of this article.